

Superconductivity in an intermetallic oxide $Hf_3Pt_4Ge_2O$

Chengchao Xu(徐程超), Hong Wang(王鸿), Huanfang Tian(田焕芳), Youguo Shi(石友国), Zi-An Li(李子安), Ruijuan Xiao(肖睿娟), Honglong Shi(施洪龙), Huaixin Yang(杨槐馨), and Jianqi Li(李建奇)
Citation: Chin. Phys. B, 2021, 30 (**7**): 077403. DOI: 10.1088/1674-1056/abfb53
Journal homepage: http://cpb.iphy.ac.cn; http://iopscience.iop.org/cpb

What follows is a list of articles you may be interested in

Substitution effect on the superconductivity in $Mo_{3-x}Re_xAl_2C$ with β-Mn structure prepared by microwave method

Jun-Nan Sun(孙俊男), Bin-Bin Ruan(阮彬彬), Meng-Hu Zhou(周孟虎), Yin Chen(陈银), Qing-Song Yang(杨清松), Lei Shan(单磊), Ming-Wei Ma(马明伟), Gen-Fu Chen(陈根富), and Zhi-An Ren(任治安)
Chin. Phys. B, 2021, 30 (**7**): 077401. DOI: 10.1088/1674-1056/abfb5a

Unusual electronic structure of Dirac material $BaMnSb_2$ revealed by angle-resolved photoemission spectroscopy

Hongtao Rong(戎洪涛), Liqin Zhou(周丽琴), Junbao He(何俊宝), Chunyao Song(宋春尧), Yu Xu(徐煜), Yongqing Cai(蔡永青), Cong Li(李聪), Qingyan Wang(王庆艳), Lin Zhao(赵林), Guodong Liu(刘国东), Zuyan Xu(许祖彦), Genfu Chen(陈根富), Hongming Weng(翁红明), and Xingjiang Zhou(周兴江)
Chin. Phys. B, 2021, 30 (**6**): 067403. DOI: 10.1088/1674-1056/ac0036

Temperature and doping dependent flat-band superconductivity on the Lieb-lattice

Feng Xu(徐峰), Lei Zhang(张磊), and Li-Yun Jiang(姜立运)
Chin. Phys. B, 2021, 30 (**6**): 067401. DOI: 10.1088/1674-1056/abdea5

Nodal superconducting gap in LiFeP revealed by NMR: Contrast with LiFeAs

A F Fang(房爱芳), R Zhou(周睿), H Tukada, J Yang(杨杰), Z Deng(邓正), X C Wang(望贤成) , C Q Jin(靳常青), and Guo-Qing Zheng(郑国庆)
Chin. Phys. B, 2021, 30 (**4**): 047403. DOI: 10.1088/1674-1056/abec37

Resistance fluctuations in superconducting $K_xFe_{2-y}Se_2$ single crystals studied by low-frequency noise spectroscopy

Hai Zi(子海), Yuan Yao(姚湲), Ming-Chong He(何明冲), Di Ke(可迪), Hong-Xing Zhan(詹红星), Yu-Qing Zhao(赵宇清), Hai-Hu Wen(闻海虎), and Cong Ren(任聪)
Chin. Phys. B, 2021, 30 (**4**): 047402. DOI: 10.1088/1674-1056/abf103

Superconductivity in an intermetallic oxide $Hf_3Pt_4Ge_2O$*

Chengchao Xu(徐程超)[1,2], Hong Wang(王鸿)[1,2], Huanfang Tian(田焕芳)[1], Youguo Shi(石友国)[1], Zi-An Li(李子安)[1], Ruijuan Xiao(肖睿娟)[1], Honglong Shi(施洪龙)[3], Huaixin Yang(杨槐馨)[1], and Jianqi Li(李建奇)[1,2,†]

[1] *Beijing National Laboratory for Condensed Matter Physics, Institute of Physics, Chinese Academy of Sciences, Beijing* 100190, *China*
[2] *School of Physical Sciences, University of Chinese Academy of Sciences, Beijing* 100049, *China*
[3] *School of Science, Minzu University, Beijing* 100081, *China*

(Received 8 April 2021; revised manuscript received 19 April 2021; accepted manuscript online 26 April 2021)

Discovery of a new superconductor with distinct crystal structure and chemistry often provides great opportunity for further expanding superconductor material base, and also leads to better understanding of superconductivity mechanisms. Here, we report the discovery of superconductivity in a new intermetallic oxide $Hf_3Pt_4Ge_2O$ synthesized through a solid-state reaction. The $Hf_3Pt_4Ge_2O$ crystallizes in a cubic structure (space group *Fm*-3*m*) with a lattice constant of $a = 1.241$ nm, whose stoichiometry and atomic structure are determined by electron microscopy and x-ray diffraction techniques. The superconductivity at 4.1 K and type-II superconducting nature are evidenced by the electrical resistivity, magnetic susceptibility, and specific heat measurements. The intermetallic oxide $Hf_3Pt_4Ge_2O$ system demonstrates an intriguing structural feature that foreign oxygen atoms can be accommodated in the interstitial sites of the ternary intermetallic framework. We also successfully synthesized a series of $Hf_3Pt_4Ge_2O_{1+\delta}$ ($-0.25 \leq \delta \leq 0.5$), and found the δ-dependent superconducting transition temperature T_c. The atomic structure and the electronic structure are also substantiated by first-principles calculations. Our results present an entirely new family of superconductors with distinct structural and chemical characteristics, and could attract research interest in further finding new superconductors and exploring novel physics pertaining to the 5d-electron in these intermetallic compound systems.

Keywords: superconductivity, intermetallic oxide, 5d-electron

PACS: 74.70.–b, 74.25.Bt, 74.25.F–, 74.25.Ha, 74.25.Jb **DOI:** 10.1088/1674-1056/abfb53

1. Introduction

Searching for new superconducting materials, in particular those of distinct structural features, has been a major endeavor since the discovery of superconductivity in mercury.[1] Discovery of a new class of superconductor often leads to significant efforts in expanding superconducting material base and furthering the understanding of superconductivity mechanisms. Prominent examples include the unexpected observation of superconductivity in $CeCu_2Si_2$ that opened the exciting field of heavy-fermion superconductors;[2] the superconducting layered cuprates, first at 35 K in Ba-doped La_2CuO_4[3] in 1986 and then at 93 K in $YBa_2Cu_3O_7$[4] in 1987, which heralded the advent of high-transition temperature superconductivity for exciting science and technology for decades; and the detection of superconductivity in 2008 in layered Fe-based compounds, LaFeAsO[5] with an $T_c \sim 26$ K, which has opened up a new opportunity in unraveling the unconventional superconducting mechanism and has offered new materials platform for exploring applications.

It is commonly acknowledged that theoretical predictions for new superconductors often meet with limited success in guiding experimental search for new superconductors. Therefore, discovery of new superconductors often relies on empirical rules[6] or systematic searching or serendipity. A favored approach is to analyze a class of crystal structure and its chemistry in which superconductors have been discovered previously, for example, the layered,[7,8] chain[9] or cage[10,11] structured compounds. Recently, several intermetallic oxides superconductors have been reported, including Nb_5Ir_3O,[13,14] Zr_5Pt_3O,[15] and Zr_4Rh_2O.[16] In these compounds, a common feature is that the intermetallic framework provides interstitial sites to accommodate the guest oxygen atoms. We explored such a distinct structure and chemistry to search for new superconductors in the intermetallic compounds. We chose to work on the Hf–Pt–Ge–O system because several RE–Pt–Ge (RE: rare earth metal) compounds[10–12] have been discovered to exhibit superconductivity. Here, we use the 5d-electron transition metal Hf to replace rare-earth elements in the hope to avoid magnetism with the superconductivity in the targeted superconductors. Additionally, we also anticipate that due to the presence of strong spin–orbit coupling in 5d-electrons[17] in Hf and Pt heavy elements, novel physics can be discovered in

*Project supported by the National Key Research and Development Program of China (Grant Nos. 2016YFA0300303, 2017YFA0504703, 2017YFA0302904, and 2017YFA0303000), the National Basic Research Program of China (Grant No. 2015CB921304), the National Natural Science Foundation of China (Grant Nos. 11774391, 11774403, and 11804381), the Strategic Priority Research Program (B) of the Chinese Academy of Sciences (Grant Nos. XDB25000000 and XDB07020000), the Scientific Instrument Developing Project of the Chinese Academy of Sciences (Grant No. ZDKYYQ20170002), and the China Postdoctoral Science Foundation (Grant No. BX20180351).

†Corresponding author. E-mail: ljq@iphy.ac.cn

© 2021 Chinese Physical Society and IOP Publishing Ltd

the new compounds.

Our initial attempts to synthesize a single phase of Hf-PtGeO with oxygen incorporated into the Hf-coordinated octahedral sites were not successful, and the resultant products were of multiphases as evidenced by x-ray diffraction (XRD), scanning electron microscopy (SEM), and energy dispersive x-ray spectroscopy (EDX) measurements. Nevertheless, some trace of superconductivity at ~ 4 K was detected by magnetic susceptibility measurements. To identify the exact superconducting phases, we employed a set of microanalysis techniques involving SEM, EDX, and transmission electron microscopy (TEM) to categorize the as-synthesized compounds by their crystallographic structures and chemical stoichiometries. A typical SEM-EDX measurement is shown in the supplementary Fig. S1. Subsequently, new syntheses were carried out by adjusting the initial ratios of the reaction precursors according to the EDX-determined stoichiometries. The products with certain stoichiometry were again checked by structural and compositional characterizations and magnetic susceptibility measurements. This approach works well and a single phase of $Hf_3Pt_4Ge_2O$ was finally identified to exhibit superconductivity at ~ 4 K. In the subsequent sections, detailed experimental determination of the crystal structure and the superconducting properties of the newly discovered intermetallic oxide $Hf_3Pt_4Ge_2O$ are presented. The atomistic and the electronic structures of $Hf_3Pt_4Ge_2O$ are also investigated by first-principles calculations to gain further insights into the structure–superconductivity correlations.

2. Experimental details

$Hf_3Pt_4Ge_2O$ polycrystalline samples have been synthesized by a conventional solid-state reaction method. The starting materials were hafnium powder (99.9%, Innochem), platinum powder (99.95%, Innochem), germanium powder (99.99%, Alfa), and HfO_2 powder (99.99%, Aladdin). Stoichiometric mixtures of the starting materials were ground and pressed into pellets, and then sealed into an evacuated quartz tube. The pellets were heated in a furnace at 850 °C for two weeks. Then the samples were slowly cooled to room temperature. The final products were found to be stable in air for months.

Magnetic susceptibility (χ) measurement was performed in a vibrating sample magnetometer (VSM, Quantum Design) from 2 K to 300 K under various applied magnetic fields in field-cooling (FC) and zero-field cooling (ZFC) modes. Measurements of electrical resistance (R) using a standard DC four-probe technique and specific heat (C_p) using a thermal relaxation method were performed from 300 K to 2 K in a physical property measurement system (PPMS, Quantum Design). Powder XRD was performed on a Bruker AXS D8 Advanced diffractometer equipped with Cu K_α radiation, and its Rietveld refinement was carried out using GSAS software.[18] Morphologies and chemical compositions of the samples were analyzed on a Hitachi model S-4800 SEM with an EDX spectrometer. Microstructures and atomic analysis were performed on an aberration-corrected transmission electron microscope (JEM-ARM200F, JEOL Inc.).

The density functional theory (DFT) simulation is adopted to investigate the electronic structure of $Hf_3Pt_4Ge_2O$. A primitive cell with 3 formula units is built as the computational model. The calculations are performed by the VASP code[19] and the generalized gradient approximation with a parameterized exchange–correlation functional according to Perdew–Burke–Ernzerhof[20] is adopted. The Hf(5p, 5d, 6s), Pt(5d, 6s), Ge(3d, 4s, 4p), and O(2s, 2p) orbitals are treated as valence states. The energy cutoffs for the plane wave basis set and augmentation charges are 520 eV and 700 eV, respectively. Both the lattice parameters and atomic sites are fully optimized on a $2 \times 2 \times 2$ k-mesh, and the total energy and electronic structures are simulated on a $3 \times 3 \times 3$ k-mesh. The energy and force convergence criteria are 10^{-5} eV and 0.01 eV/Å, respectively. Both the band structure and density of states without and with spin–orbit coupling are considered for bulk $Hf_3Pt_4Ge_2O$.

3. Results and discussion

To identify new superconductors in the as-synthesized multiphase Hf–Pt–Ge–O samples that initially exhibited trace of superconductivity at ~ 4 K by magnetic susceptibility, we used the SEM-EDX method to analyze the crystallite morphologies and compositions. Subsequent syntheses adopted with the determined stoichiometries were conducted to finally isolate the superconducting phase by magnetic susceptibility; the stoichiometry of the superconducting $Hf_3Pt_4Ge_2O$ and its typical morphologies of multi-faceted gains were obtained by the SEM-EDX measurements, as shown in the inset to Fig. 1(c). Since crystal database search and literature survey find no such record of $Hf_3Pt_4Ge_2O$ compound, we conclude that a new intermetallic oxide $Hf_3Pt_4Ge_2O$ superconductor has been synthesized.

We combined both powder XRD and TEM measurements to determine the crystal structure of $Hf_3Pt_4Ge_2O$. For this new crystal phase, we determined the crystal unit cell (Bravais lattice) of $Hf_3Pt_4Ge_2O$ to be face-centered cubic with $a = 1.2411$ nm through analysis of series of electron diffraction patterns (shown in supplementary Fig. S2). Figure 1(a) shows a typical [100]-oriented electron diffraction pattern, and Fig. 1(b) shows the atomically resolved Z-contrast image of the [100]-oriented $Hf_3Pt_4Ge_2O$ thin specimen. A few major, low-indexed zone-axis atomic images are used to derive the crystallographic Wyckoff sites for the constituent heavy elements (Hf, Pt, Ge) in a specific space group. However, ow-

ing to the weak scattering strength of oxygen, accurate determination of crystallographic sites for oxygen is challenging via XRD measurement. Alternatively, according to the rule of elementary electronegativity (the tendency of an atom to attract electrons towards this atom) for Hf(1.3) < Ge(2.01) < Pt(2.28), we rationalize that oxygens are bonded with low electronegativity Hf and Ge within the intermetallic Hf–Pt–Ge framework. In addition, we also carried out extensive first-principles calculation on the possible crystallographic setting for oxygen in the Hf–Pt–Ge framework. The initial derived atomic positions can then be refined by the Rietveld refinement of powder XRD data. Figure 1(c) shows the measured powder XRD profile and its Rietveld refinement, yielding a crystal structure with space group *Fm*-3*m* and a lattice constant of 1.2411 nm. It is note that the refinement values of $R_p = 13\%$ and $R_{wp} = 8\%$ are relatively high, likely due to the preferential growth of certain lattice planes and the presence of additional impurity phases. We note that accurate determination of the atomic positions of oxygen in $Hf_3Pt_4Ge_2O$ can be achieved in future study via advanced synchrotron x-ray or neutron scattering measurements on samples of improved crystallinity.

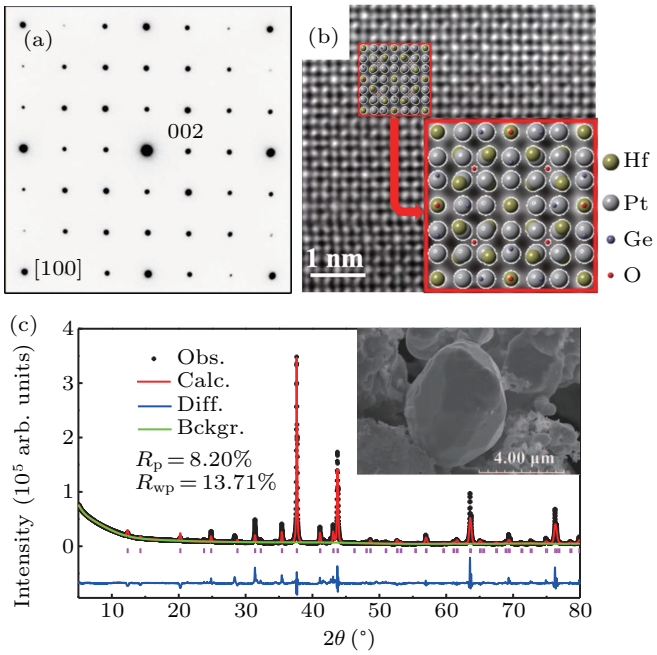


Fig. 1. Determination of crystal structure and stoichiometry of $Hf_3Pt_4Ge_2O$ using TEM and powder XRD. (a) [100]-oriented electron diffraction. (b) *Z*-contrast atomic image via high-angle annual dark-field HAADF imaging. Red frame marks the [100]-projected unit cell dimension. (c) Powder XRD profile and its Rietveld refinement. Inset shows a SEM image of $Hf_3Pt_4Ge_2O$ crystalline grains.

Analyses of the combined TEM and powder XRD measurements have revealed that $Hf_3Pt_4Ge_2O$ crystalizes in a face-centered cubic structure with a space group *Fm*-3*m* (No. 225). Figure 2 depicts the atomic representation of intermetallic oxide $Hf_3Pt_4Ge_2O$, in which a total of 120 atoms are accommodated in a conventional unit cell with a molecule formula number $Z = 12$. In *Fm*-3*m* setting, Ge atoms occupy the Wyckoff positions 24e, Pt atoms occupy 48i, Hf atoms are divided into two Wyckoff positions of 32f for Hf(I) and 4a for Hf(II), and O atoms also occupy two Wyckoff positions of 8c for O(I) and 4b for O(II).

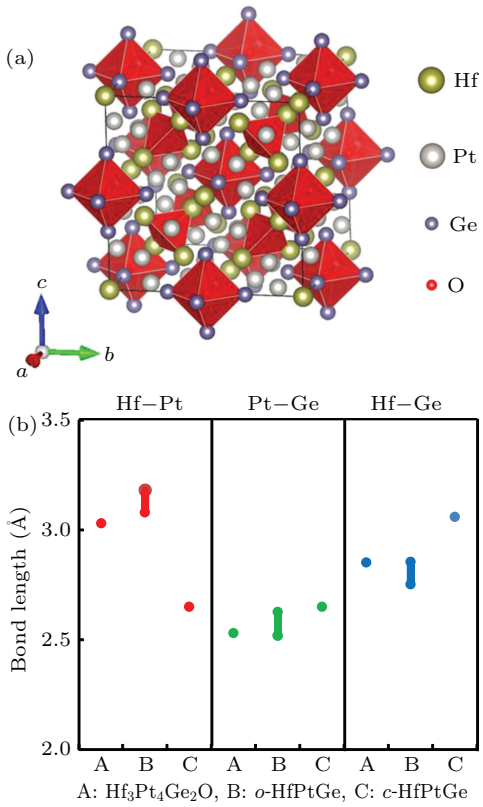


Fig. 2. Crystal structure of the intermetallic oxide $Hf_3Pt_4Ge_2O$. (a) side view of the unit cell of cubic $Hf_3Pt_4Ge_2O$. O(I) are tetrahedrally-coordinated 4 Hf(I) atoms, while O(II) are octahedrally-coordinated by 8 Ge atoms. (b) Bond lengths of Hf–Pt, Pt–Ge, and Hf–Ge in the new intermetallic oxide $Hf_3Pt_4Ge_2O$ and two typical HfPtGe intermetallic compounds of cubic *c*-HfPtGe with *F*-43*m* and orthorhombic *o*-HfPtGe with (*Pnma*). Note the similar bond lengths in $Hf_3Pt_4Ge_2O$ and *o*-HfPtGe, which are both of metallic characters, while *c*-HfPtGe is a semiconductor with energy gap ~ 1 eV.

A summary of the atomic coordinates of cubic $Hf_3Pt_4Ge_2O$ is listed in Table 1, together with the determined lattice parameters and the Rietveld refinement values. In this newly discovered crystal structure, two unique features are prominent: the Hf–Pt–Ge intermetallic framework and the interstitial sites for oxygen atoms. As shown in Fig. 2(b), the $Hf_3Pt_4Ge_2O$ intermetallic builds a cubic framework with their respective bond lengths of Pt–Ge ~ 0.253 nm, Hf(I)–Ge ~ 0.285 nm, and Hf–Pt ~ 0.303 nm. Figure 2(b) presents an informative comparison for the chemical bond characteristics of the Hf–Pt–Ge intermetallics, in which the bond lengths of $Hf_3Pt_4Ge_2O$ are similar to those of the high-temperature orthorhombic phase of HfPtGe[21] with a space group *Pnma* (designated as *o*-HfPtGe). Note that a low-temperature cubic phase HfPtGe[22] with *F*-43*m* (designated as *c*-HfPtGe) was recently discovered, which is a semiconductor with a band gap about ~ 1 eV. It is noted that foreign oxygen atoms are readily

incorporated into the interstitial sites provided by the Hf–Pt–Ge intermetallic framework. Specifically, the O(I) at Wyckoff site 8c is coordinated by 4 nearest-neighboring Hf(I) at 32f sites to form O(I)–Hf(I) tetrahedra, while the O(II) at 4b sites is coordinated by 8 nearest-neighboring Ge to form O(II)–Ge octahedra. It is noteworthy that the bond length of O(I)–Hf(I) is about 0.210 nm, which is of ionic character, while the bond length of O(II)–Ge is about 0.278 nm, which is indicative of weakly covalent bonds (see also the results in first-principles calculations below).

Table 1. Crystal data and atomic coordinates of $H_3Pt_4Ge_2O$ at 300 K.

Atom	Wyckoff position	Occupation	x	y	z	U_{iso}
Hf1	32f	1	0.35013(15)	0.35013(15)	0.35013(15)	0.00666
Hf2	4a	1	0	0	0	0.0043(32)
Pt	48i	1	0	0.17196(17)	0.17196(17)	0.0074(5)
Ge	24e	1	0.2955(9)	0	0	0.053(4)
O1	8c	1	1/4	1/4	1/4	0.09
O2	4b	1	1/2	1/2	1/2	0.09

Empirical formula: $Hf_3Pt_4Ge_2O$, space group: Fm-3m (No. 225), $Z = 12$.
Lattice parameter: $a = 12.41188(12)$ Å, $R_{wp} = 13.71\%$, $R_p = 8.2\%$.

The temperature-dependent DC magnetic susceptibility of $Hf_3Pt_4Ge_2O$ was measured in an applied magnetic field of 10 Oe between 2 K to 300 K in zero-field-cooling (ZFC) and field-cooling (FC) modes. A strong diamagnetic signal of superconducting transitions appears at the critical temperature $T_c = 4.24$ K as shown in Fig. 3(a). Figure 3(b) shows a series of field-dependent magnetization $M(H)$ curves with H ranging from 0 Oe to 1000 Oe and temperature between 2 K to 5 K. It is well known that determining precisely the lower critical field H_{c1} from $M(H)$ measurement is challenging, especially for polycrystalline samples. As a criterion, we here used the identification of H_{c1} as the magnetic field where $M(H)$ first deviates from linearity. A reasonable estimation of $H_{c1}(0) \approx 39.7$ Oe can be obtained by using the empirical formula[23] $H_{c1}(T) = H_{c1}(0)[1-(T/T_c)^2]$. Because of the high purity of the main phase, it can be considered that the superconducting volume fraction at 2 K is 100%, which means complete diamagnetism and the magnetic susceptibility equals -1. The $4\pi\chi$–T curve measured in ZFC mode shows that the magnetic susceptibility at 2 K is -1.39, thus the demagnetization factor $N = 0.281$ can be obtained from $4\pi\chi(1-N) = -1$. Finally, we obtain the modified $H_{c1}(0) = 39.7$ Oe$/(1-N) = 55.18$ Oe.

Figure 3(c) shows the temperature-dependent normalized electrical resistance ($R(T)/R(300\ \mathrm{K})$) from 2 K to 300 K under zero magnetic field in $Hf_3Pt_4Ge_2O$ measured by standard four-probe method. In general, the resistance of this superconducting phase shows a metallic behavior decreasing with lowering temperature above T_c. A sharp superconducting transition is observed at the onset temperature at 4.24 K and zero resistivity occurs below 3.96 K, giving a superconducting transition width of $\Delta T_c \approx 0.27$ K. In order to obtain the upper critical field $H_{c2}(0)$ the commonly used 50% criterion was chosen, which corresponds to the midpoints of the series $R(T)$ curves in a range of external magnetic fields between 0 to 1500 Oe, as shown in the inset to Fig. 3(c). Figure 3(d) exhibits the extrapolated slopes near T_c, $\mathrm{d}H_{c2}/\mathrm{d}T = -9492.7$ Oe/K. we can obtain that $H_{c2}(0) \approx 2.76$ T, according to the Werthamer–Helfand–Hohenberg (WHH) formula $H_{c2}^{WHH}(0) = -0.693T_c(\mathrm{d}H_{c2}/\mathrm{d}T)_{T=T_c}$.[24]

Figure 3(e) shows the temperature-dependent specific heat capacities $C_p(T)$ of $Hf_3Pt_4Ge_2O$ measured from 2 K to 8 K in zero-field. In the C_p/T vs. T plot, a clear specific heat jump occurs at ~ 4.1 K, which marks the onset temperature of superconducting transition. The electron specific heat coefficient (γ) and phonon specific heat coefficient (β) are also estimated by nonlinear fitting: $C/T = \gamma + \beta T^2$, $\gamma_e \approx 15.70$ mJ·mol^{-1}·K^{-2}, $\beta \approx 2.13$ mJ·mol^{-1}·K^{-4}. It is also noted that the specific heat jump signal of the sample is relatively weak, due to the low densification of this polycrystalline sample. It is well established that the specific heat jump $\Delta C_e/\gamma T_c$ value around 1.43 is based on s-wave pairing under the weak coupling of BCS theory. However, in some superconductor systems, this value was found to differ considerably from 1.43. Theoretically, even the phonon-mediated BCS superconductors do not necessarily hold this particular value of 1.43. For example, the theoretical jump value of weak coupling d-wave superconductor is around 0.9,[25] which is much smaller than 1.43. Second, the specific heat measurement can be affected by extrinsic effects, such as the density of the sample and the poor thermal conductivity in coarsely-grained polycrystalline samples. In addition, such a small value has also been observed in some intermetallic compound superconductors and iron-based superconductors, such as $Zr_5Ge_{2.5}Ru_{0.5}$,[26] FeS,[27] and KFe_2As_2,[28] and also for the p-wave superconductor Sr_2RuO_4.[29] Therefore, the unexpected low value of specific heat jump measured in our $Hf_3Pt_4Ge_2O$ may be associated with extrinsic effects of sample quality and/or intrinsic unconventional superconductivity that is not described by weak coupling BCS theory, which requires further investigations.

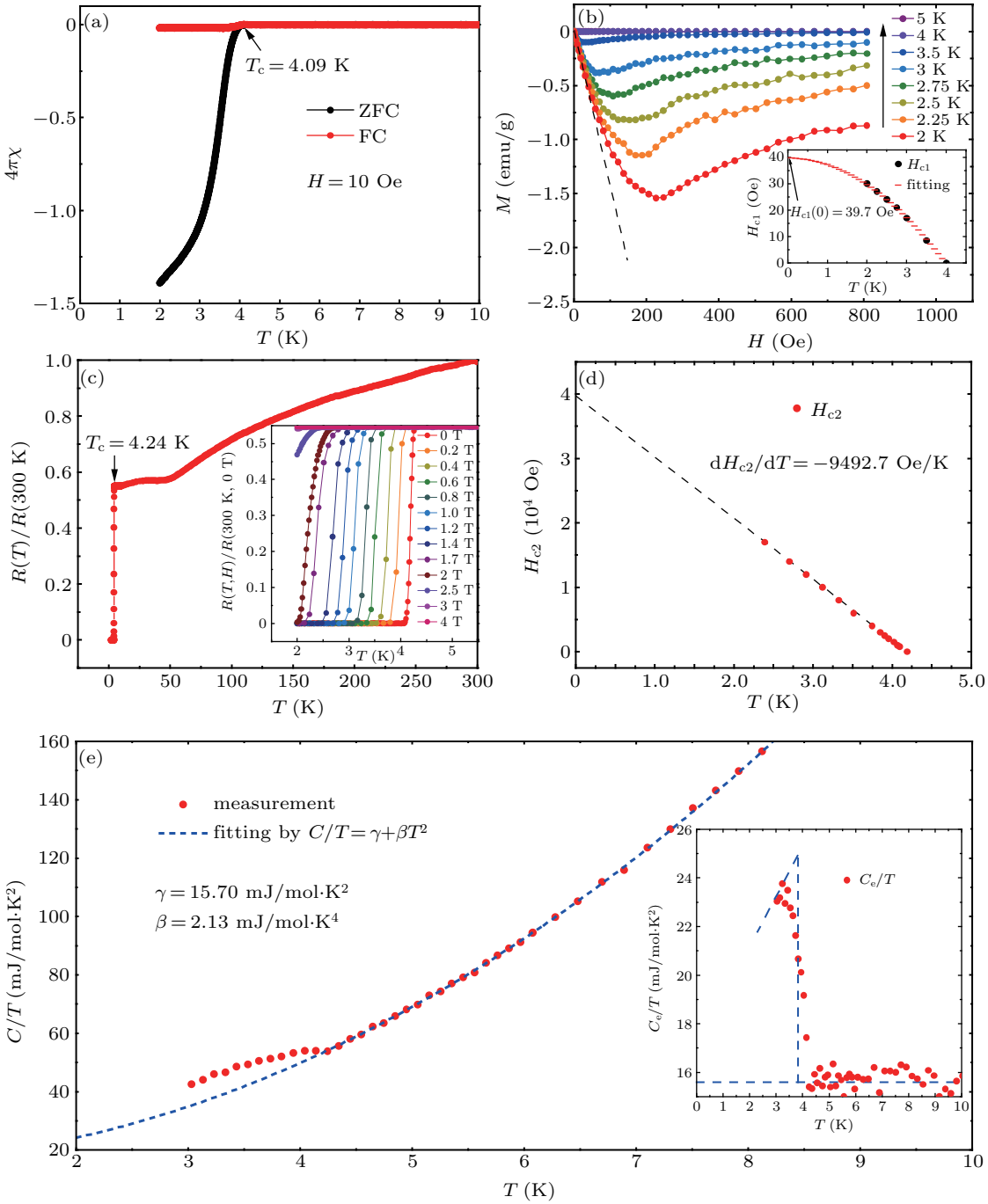


Fig. 3. Superconductivity at ~ 4 K in $Hf_3Pt_4Ge_2O$ is evidenced by the temperature and field dependence of magnetic susceptibility $\chi(T,H)$, electrical resistivity $R(T,H)$, and specific heat $C_p(T)$. (a) $\chi(T)$ measured in zero-field cooling (ZFC) and 10 Oe-field cooling (FC) modes. (b) Determination of the lower critical field (uncorrected for demagnetization factor) $H_{c1} \sim 39.7$ Oe by low-field magnetization curves at various applied fields, $M(T,H)$. (c) Temperature-dependent resistivity measured from 300 K to 2 K in zero-field, and inset shows field-dependent resistivity measured in a temperature range 2–5 K under various fields from 0 to 4 T. (d) The field-dependent resistivity data are used to determine the upper critical field $H_{c2} \sim 2.76$ T. (e) Specific heat measurement shows a clear jump at 4 K that is associated with superconducting transition. Inset shows the electronic contribution to specific heat over temperature $C_e(T)/T$ via an equal-area construction method.

The Debye temperature is estimated to be $\Theta_D = 209$ K, using the relationship $\beta = (12\pi^4/5)nR/\Theta_D^3$, where n is the atom number in a formula unit and R is the gas constant. From the McMillan formula[30] $T_c = \left(\frac{\Theta_D}{1.45}\right)\exp[-1.04(1+\lambda_{e-p})]/[\lambda_{e-p} - \mu^*(1+0.62\lambda_{e-p})]\}$, together with the assumed Coulomb pseudopotential,[31] $\mu^* = 0.15$, the electron–phonon coupling constant is estimated to be $\lambda_{e-p} = 0.68$, indicating a weakly coupled superconductor. The above evaluated superconducting parameters are tabulated in Table 2.

Microstructural and chemical analyses for these samples reveal that only a small fraction of HfO_2 remains in the final product, which is a nonmagnetic insulator. The starting materials contain elemental Hf metal which is the only possible elemental superconductor with $T_c < 0.4$ K.[32] These facts indicate that the superconductivity is solely attributed to the newly-determined cubic phase of $Hf_3Pt_4Ge_2O$. In addition,

we synthesized a series of samples with different oxygen content through varying the amount of HfO_2 powder in the starting precursor materials but keeping reaction conditions unchanged. It was anticipated that in the Hf–Pt–Ge intermetallic framework, the oxygen contents at their interstitial sites can be regulated as $Hf_3Pt_4Ge_2O_{1+\delta}$ with nominal $\delta = -0.25$, -0.125, 0, $+0.125$, $+0.25$, $+0.5$. The as-synthesized series of $Hf_3Pt_4Ge_2O_{1+\delta}$ samples were characterized by powder XRD, as seen in supplementary Fig. S3. Though a small fraction impurity phase can be observed in superconducting samples, particular those with $\delta > 0.125$, our resistivity and magnetic susceptibility measurements (supplementary Fig. S4) clearly show a trend in the transition temperature T_c: a decreasing in T_c with stoichiometric deviation δ. This fact suggests that the presence of atomic interstitials and the relevant local structural variations may allow certain regulations for electronic structures of $Hf_3Pt_4Ge_2O_{1+\delta}$ compounds, thereby enabling a greater electronic tunability. We also experimentally observe a non-monotonic relationship between the T_c and the oxygen content $(1+\delta)$ in the intermetallic oxide $Hf_3Pt_4Ge_2O_{1+\delta}$. Such a non-monotonic T_c vs. $(1+\delta)$ may be associated with the intercalated oxygen atoms occupying two distinct crystallographic sites and the preferential formation of oxygen vacancies or interstitials in specific crystallographic sites. Understanding the role of interstitial oxygen on the superconductivity mechanisms and its dependence on T_c in the intermetallic oxide $Hf_3Pt_4Ge_2O_{1+\delta}$ needs further investigation.

Table 2. Summary of superconducting parameters of $H_3Pt_4Ge_2O$.

Parameter	$H_3Pt_4Ge_2O$
T_c (K) (via specific heat)	4.1
$H_{c1}(0)$ (mT)	5.52
$H_{c2}(0)$ (T)	2.76
γ_e (mJ/mol·K^2)	15.70
β (mJ/mol·K^4)	2.13
Θ_D (K)	208.87
$\xi(0)$ (Å)	109.20
$\lambda(0)$ (Å)	1130.22
κ	10.35
H_c (mT)	80.75
$\Delta C_e/\gamma_e T_c$	0.60
λ_{e-p}	0.68

Here we elucidate the important role of the intercalating oxygen in stabilizing the $H_3Pt_4Ge_2O$ crystal phase. We attempted to synthesize a nominal $H_3Pt_4Ge_2$ with no inclusion of oxygen element from the precursors but kept the synthesis conditions (reaction temperature, duration time, etc.) identical. We found that the nominal $H_3Pt_4Ge_2$ cannot be obtained, instead, the final products are mainly comprised of cubic-type *c*-HfPtGe and orthorhombic-type *o*-HfPtGe, as clearly seen in the XRD data in Fig. 4(a). We then measured the magnetic susceptibility of the nominal $H_3Pt_4Ge_2$ and found a tiny superconducting signal of $H_3Pt_4Ge_2$ appearing at ~ 4 K (see Fig. 4(b)), which can be attributed to the small trace of $H_3Pt_4Ge_2O$. The shielding fraction of the $H_3Pt_4Ge_2$ sample is less than 0.5% that of $H_3Pt_4Ge_2O$. Such a small trace of $H_3Pt_4Ge_2O$ is inevitable as the used elementary precursors (Hf, Pt, Ge) are naturally surface-layer-oxidized.

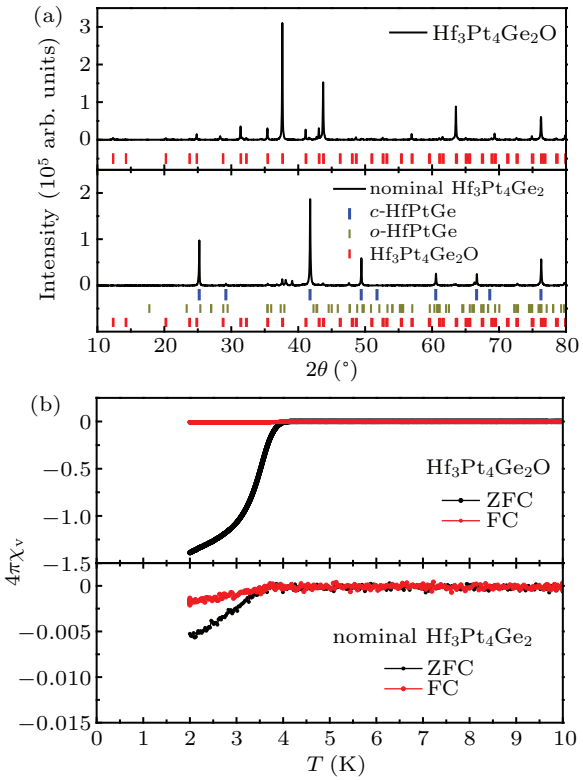


Fig. 4. (a) XRD profiles for new intermetallic oxides $H_3Pt_4Ge_2O$ in upper panel and the nominal $H_3Pt_4Ge_2$ in lower panel. (b) Magnetic susceptibility for new intermetallic oxides $H_3Pt_4Ge_2O$ in upper panel and the nominal $H_3Pt_4Ge_2$ in lower panel.

The electronic structure of $Hf_3Pt_4Ge_2O$ is simulated with and without spin–orbit coupling (SOC), as shown in Fig. 5. The optimized cell shows lattice length of 1.2536 nm, which is very close to the experimental value of 1.2411 nm. A metallic ground state is observed in the band structure of $Hf_3Pt_4Ge_2O$, which is consistent with the electrical resistivity measurement. Along the *W*–*L* direction, one band close to the Fermi level shifts downwards for ~ 0.04 eV because of the spin–orbit coupling, the band composition analysis indicates that it is mainly attributed by Pt 5d (25%), Hf 5d (21%), and O 2p (11%) orbitals. Obvious band splits are observed at Γ points when SOC is included. At Γ point, the band around 0.4 eV above the Fermi level composed of Hf 5d (39%) and Pt 5d (22%) splits ~ 0.2 eV. The density of states considering SOC indicates that the mainly contributions around the Fermi level are Pt 5d and Hf 5d orbitals, and the hybridization between Ge 3p and O 2p orbitals confirms the covalent characteristics of Ge–O bond. Several van Hove singularities can be found near the Fermi level, which is thought as a good precondition for superconductivity as what found in Heusler compound.[33]

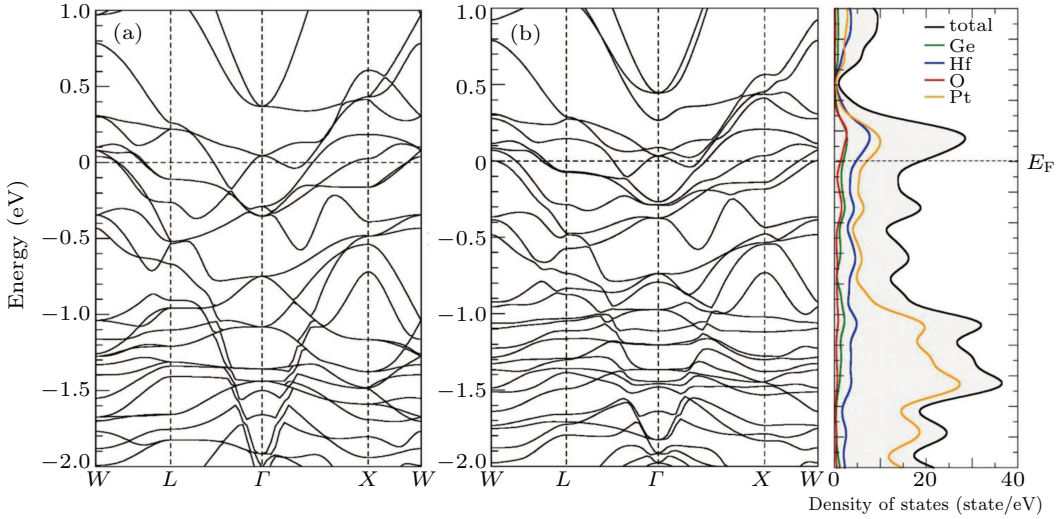


Fig. 5. Electronic band structures of $Hf_3Pt_4Ge_2O$ (a) without and (b) with the spin–orbit coupling and the density of state (DOS) by first-principles calculations.

Our new superconducting compound $Hf_3Pt_4Ge_2O$ owns its specific term as an intermetallic oxide, which presents its distinct structural and stoichiometric characteristics in comparison to the intermetallic-type and the omnipresent perovskite-type oxide superconductors. In intermetallics superconductors, classical systems include the Nb_3Sn[34] and Nb_3Ge[35] that crystalize in A15-type cubic structure, the $RbCs_2C_{60}$,[36] the YNi_2B_2C,[37] and the MgB_2.[38] Recently, Heusler-type intermetallics superconductors also attracted considerable attention (see the review[33] and the references therein). In these intermetallics systems, the constituent elements are metals or metalloids and their chemical bonds are of metallic and covalent nature. By contrast, for oxides superconductors, notably the layered cuprate and the derivatives,[39] oxygen anions form the structural framework to afford octahedrally- and/or tetrahedrally-coordinated interstitial sites for metallic cations. The new $Hf_3Pt_4Ge_2O$ intermetallic oxide superconductor is unique for its intermetallic framework comprised of metallic and covalent bonds, and for its interstitial sites for accommodating oxygen anions of ionic character. Therefore, subsequent efforts are anticipated to be directed to finding new intermetallic oxides superconductors and to exploring novel physics associated with their complex nature of chemical bonds and the strong spin–orbit coupling effects intrinsic to heavy elements.

4. Conclusion

In summary, using solid-state reaction method, we have synthesized a new intermetallic oxide $Hf_3Pt_4Ge_2O$ superconductor with a transition temperature at ~ 4.1 K. We combined the microanalysis techniques of electron microscopy (TEM, SEM, and EDX) and the Rietveld refinement of powder x-ray diffraction to determine the crystal structure and chemical stoichiometry of $Hf_3Pt_4Ge_2O$. The structural analyses reveal that $Hf_3Pt_4Ge_2O$ crystallizes in a cubic structure of space group *Fm*-3*m* with a lattice constant of $a = 1.2411$ nm at room temperature, and features a Hf–Pt–Ge intermetallic network with oxygen atoms occupying the interstitial sites tetrahedrally-coordinated by Hf(I) and octahedrally-coordinated by Ge. We then used the electrical resistivity, magnetic susceptibility, and specific heat measurements to evaluate the superconducting properties of $Hf_3Pt_4Ge_2O$ superconductor, as tabulated in Table 2. According to these parameters, $Hf_3Pt_4Ge_2O$ exhibits bulk, type-II superconductivity and the BCS electron–phonon picture is applicable to describe the superconductivity in $Hf_3Pt_4Ge_2O$. We further employed first-principles calculations to gain insights into the atomistic stability and electronic band structure of $Hf_3Pt_4Ge_2O$, and the theoretical calculations reveal the splitting of Pt 5d and Hf 5d bands caused by spin–orbit coupling, as well as the appearance of van Hove singularities in the vicinity of the Fermi energy that is believed to be a conducive factor for superconductivity.

Despite the relatively low T_c at ~ 4.1 K, the $Hf_3Pt_4Ge_2O$ is an entirely new superconducting compound with prominent structural and chemical characteristics. Firstly, in this new compound, a Hf–Pt–Ge intermetallic network offers interstitial sites to accommodate guest atoms such as oxygen of large electronegativity. Secondly, a mixed chemical bonding nature involves bonds of metallic Hf–Pt, covalent Hf–Ge, Pt–Ge, and Ge–O, and ionic Hf–O. Thirdly, the involvement of heavy 5d-electron transition metals Hf and Pt leads to strong spin–orbit coupling in the electronic structure. These distinct structural characteristics might permit incorporation of other types of foreign atoms such as nitrogen and fluorine. Given the vast choice of 4d, 5d transition metals and their combination, we anticipate that a large number of new intermetallic oxides, fluorides, and nitrides can be obtained and some of them might exhibit superconductivity with even higher transition temperatures.

Acknowledgments

We thank Dr. Menghu Zhou for his assistance in Rietveld refinement of XRD data, thank Dr. Hua Zhang and Pro. Xiaoli Dong for their assistance in PPMS measurement.

References

[1] Onnes H K 1911 *Comm. Phys. Lab. Univ. Leiden* **28** 120
[2] Steglich F, Aarts J, Bredl C D, Lieke W, Meschede D, Franz W and Schaefer H 1979 *Phys. Rev. Lett.* **43** 1892
[3] Bednorz J G and Müller K A 1986 *Z. Phys. B* **64** 189
[4] Wu M K, Ashburn J R, Torng C J, Hor P H, Meng R L, Gao L, Huang Z J, Wang Y Q and Chu C W 1987 *Phys. Rev. Lett.* **58** 908
[5] Kamihara Y, Watanabe T, Hirano M and Hosono H 2008 *J. Am. Chem. Soc.* **130** 3296
[6] Matthias B T 1970 *The Empirical Approach to Superconductivity* (Boston: Springer)
[7] Morosan E, Zandbergen H W, Dennis B S, Bos J W G, Onose Y, Klimczuk T, Ramirez A P, Ong N P and Cava R J 2006 *Nat. Phys.* **2** 544
[8] Mao Y Y, Li J, Huan Y L, Yuan J, Li Z A, Chai K, Ma M W, Ni S L, Tian J P, Liu S B, Zhou H X, Zhou F, Li J Q, Zhang G M, Jin K, Dong X L and Zhao Z X. 2018 *Chin. Phys. Lett.* **35** 057402
[9] Bao J K, Liu J Y, Ma C W, Meng Z H, Tang Z T, Sun Y L, Zhai H F, Jiang H, Bai H, Feng C M, Xu Z A and Cao G H 2015 *Phys. Rev. X* **5** 011013
[10] Gumeniuk R, Schnelle W, Rosner H, Nicklas M, Leithe J A and Grin Y 2008 *Phys. Rev. Lett.* **100** 017002
[11] Zang J W, Zhang J, Zhu Z H, Ding Z F, Huang K, Peng X R, Hillier A D and Shu L 2019 *Chin. Phys. Lett.* **36** 107402
[12] Sheng Q, Zhang J, Huang K, Ding Z, Peng X, Tan C and Shu L 2017 *Chin. Phys. B* **26** 057401
[13] Zhang Y, Wang B, Xiao Z, Lu Y, Kamiya T, Uwatoko Y, Kageyama H and Hosono H 2017 *npj Quantum Materials* **2** 45
[14] Wang B, Zhang Y Q, Xu S X, Ishigaki K, Matsubayashi K, Cheng J G, Hosono H and Uwatoko Y. 2019 *Chin. Phys. B* **28** 107401
[15] Hamamoto S and Kitagawa J 2018 *Mater. Res. Express* **5** 106001
[16] Ma K, Lago J and Rohr F O V 2019 *J. Alloys Compd.* **796** 287
[17] Liu Z, Wu W, Zhao Z, Zhao H, Cui J, Shan P, Zhang J, Yang C, Sun P, Wei Y, Li S, Zhao J, Sui Y, Cheng J, Lu L, Luo J and Liu G 2019 *Phys. Rev. B* **99** 184509
[18] Larson A C and Dreele R B V 2000 *Los Alamos National Laboratory Report LAUR* **86**
[19] Kresse G and Joubert D 1999 *Phys. Rev. B* **59** 1758
[20] Kresse G and Furthmüller J 1996 *Phys. Rev. B* **54** 11169
[21] Nagata Y, Sodeyama K, Yashiro S, Sasaki H, Samata H, Uchida T and Lan M D 1998 *J. Alloys Compd.* **281** 112
[22] Bende D, Wagner F R, Sichevych O and Grin Y 2017 *Angew. Chem. Int. Ed.* **56** 1313
[23] Brandt E H 2004 *Physica C* **404** 74
[24] Helfand E and Werthamer N R 1966 *Phys. Rev.* **147** 288
[25] Xiang T 2006 *d-Wave Superconductivity* (Beijing: Science Press) pp. 55–56 (in Chinese)
[26] Li S, Liu X Y, Anand V and Bing Lv 2018 *New. J. Phys.* **20** aa9ccd
[27] Xing J, Lin H, Li Y F, Li S, Zhu X Y, Yang H and Wen H H. 2016 *Phys. Rev. B* **93** 104520
[28] Hafiez M A, Aswartham S, Wurmehl S, Grinenko V, Hess C, Drechsler S L, Johnston S, Wolter A U B, Büchner B, Rosner H and Boeri L. 2012 *Phys. Rev. B* **85** 134533
[29] Deguchi K, Mao Z Q, Yaguchi H and Maeno Y 2004 *Phys. Rev. Lett.* **92** 047002
[30] McMillan W L 1968 *Phys. Rev.* **167** 331
[31] Wang B and Ohgushi K 2013 *Sci. Rep.* **3** 3381
[32] Hein R A 1956 *Phys. Rev.* **102** 1511
[33] Klimczuk T, Wang C H, Gofryk K, Ronning F, Winterlik J, Fecher G H, Griveau J C, Colineau E, Felser C, Thompson J D, Safarik D J and Cava R J 2012 *Phys. Rev. B* **85** 174505
[34] Matthias B T, Geballe T H and Corenzwit E 1954 *Phys. Rev.* **95** 143
[35] Matthias B T, Geballe T H, Longinotti L D, Corenzwit E, Hull G W, Willens R H and Maita J P 1967 *Science* **156** 645
[36] Tanigaki K, Ebbesen T W, Saito S, Mizuki J, Tsai J S, Kubo Y and Kuroshima S 1991 *Nature* **352** 222
[37] Cava R J, Takagi H, Zandbergen H W, Krajewski J J, Peck W F, Siegrist T, Batlogg B, Dover R B V, Felder R J, Mizuhashi K, Lee J O, Eisaki H and Uchida S 1994 *Nature* **367** 252
[38] Nagamatsu J, Nakagawa N, Muranaka T, Zenitani Y and Akimitsu J 2001 *Nature* **410** 63
[39] Cava R J 2000 *J. Am. Ceram. Soc.* **83** 5